# Femtosecond laser plasma plume characteristics in the nanojoule ablation regime

S. P. Banerjee, Zhijiang Chen, and R. Fedosejevs

Citation: Journal of Applied Physics **113**, 183101 (2013); doi: 10.1063/1.4804329
View online: http://dx.doi.org/10.1063/1.4804329
View Table of Contents: http://scitation.aip.org/content/aip/journal/jap/113/18?ver=pdfcov
Published by the AIP Publishing



# Femtosecond laser plasma plume characteristics in the nanojoule ablation regime

S. P. Banerjee,[a] Zhijiang Chen, and R. Fedosejevs
*Department of Electrical and Computer Engineering, University of Alberta, Edmonton, Alberta T6G2V4, Canada*

(Received 5 March 2013; accepted 24 April 2013; published online 9 May 2013)

Laser ablation of chromium with nanojoule energy UV femtosecond pulses under background pressure conditions between 0.3 Torr and 700 Torr is studied and the corresponding plasma plume images at different times after irradiation are measured. The ablation focal spot is less than or the order of a micron when 170 nJ of laser pulse energy is used. This low pulse energy leads to short lifetimes of the plasma of the order of tens of nanoseconds. The plume shape changes with ambient pressure due to the collision with background gas. An axially stretched plume changes to a more circular plume as the pressure increases. In addition, a separation of the ionic and atomic components is observed at lower pressure. These two components move at significantly different velocities as well. The plasma plume expands at almost constant velocity at very low pressure but exhibits significant deceleration at higher pressure reaching an asymptotic stopping distance. Plume images are also obtained near the ablation threshold pulse energy. The plume characteristics are compared to different models of plume expansion. © *2013 AIP Publishing LLC*. [http://dx.doi.org/10.1063/1.4804329]

## I. INTRODUCTION

Understanding laser ablation physics and the behavior of plasma plume expansion in the case of ultrashort femtosecond laser pulses is quite important in pulsed laser deposition,[1,2] laser micromachining, laser material processing,[3–6] nanoparticle synthesis,[7] and nanoparticle deposition as well as laser induced breakdown spectroscopy (LIBS).[8,9] Laser ablation and the evolution of laser ablated plasmas are complex phenomena in the time and space domains. The characteristic parameters of a laser produced plasma change with laser irradiation and ambient pressure conditions. Altering the background gas pressure changes the collision rate and affects the expansion of the plasma plume. In addition to changing the size and shape of a laser produced plasma, lower background pressure enhances the emission signal intensity significantly.[10] Plume dynamics is important in pulsed laser deposition as it determines the growth and quality of a thin film deposited in background gases. In general, lower background pressure helps improve material processing as well. In a study of the ablation plume, it is important to measure the different components of a plume (e.g., ionic, atomic, and nanoparticle), their behavior, and their dependence on different parameters. Various studies related to plasma plume expansion in background gases using nanosecond lasers have been reported.[11–16] Kagawa and Yokoi[11] first obtained images of plasmas when a nitrogen laser was focused on the surface of a copper plate under different background pressure conditions. The authors reported that the diameter of the plasma plume as well as characteristic emission spectra varied with gas pressures. They also identified two distinct plasma regions at low pressure (1 Torr). Femtosecond laser pulses interact with plasmas on a very short time scale and limited spatial scale. The investigation of plasma plumes generated by femtosecond laser pulses has been a topic of significant interest in the last several years. Experiments on the dynamics of the plasma plume created with femtosecond laser pulses have been reported by a number of authors in recent years.[17–22] Amoruso *et al.* have carried out investigations on propagation dynamics of the different components of femtosecond plasma plume such as the atomic and nanoparticle plumes[18,19] and angular distributions of plume components.[23] Canulescu *et al.*[20] have compared nanosecond and femtosecond ablation plume dynamics. Most of the reported experiments were carried out using laser pulse energies of tens of microjoules or more. Plasmas generated with much lower incident laser pulse energies will have shorter lifetimes and small propagation lengths. If a very small focal spot size is employed, for example, by using a high numerical aperture objective to focus the laser pulses, then the spatial structure of the plasma plume will also be much smaller. Working in the UV wavelength range enables submicron focal spots and at the same time leads to enhanced absorption of laser pulse energy on most target materials. Such conditions would be optimal for carrying out high precision material processing with ultrafast lasers. Therefore, it is important to understand the behavior of plasma plumes generated by low energy, tightly focused UV laser pulses. In the current investigation, we study the characteristics of the plasma plume generated by 266 nm femtosecond laser pulses with 26–170 nJ energy. A microplasma is produced by such ultrashort femtosecond laser pulses by focusing to submicron focal spots. The evolution and the dynamics of the plasma plume expansion at different background pressures are discussed in Secs. III–V.

[a]Electronic mail: shyama.banerjee@gmail.com

 

## II. EXPERIMENTAL PROCEDURE

The experimental setup used for this experiment is shown in Fig. 1. A Ti:sapphire (Spectra-Physics Hurricane) laser was used for our study to generate ~120 fs (FWHM) pulses at 800 nm with the maximum energy ~600 $\mu$J. We have used a half-wave plate and a Glan polarizer to control the output laser pulse energy. Part of the main pulse was then frequency doubled by using a BiBO nonlinear crystal to 400 nm. The maximum pulse energy obtained for the 400 nm pulse was ~120 $\mu$J. A frequency tripled laser pulse of 266 nm was generated by the use of an additional BBO crystal through mixing both 800 nm and 400 nm under phase matched conditions. The output from the third harmonic crystal (BBO) contains contributions from the source 800 nm pulses and the second harmonic 400 nm pulses. Dichroic mirrors and spatial filtering of the final pulse were employed to get rid of unwanted wavelength components in the beam and transmit only the 266 nm pulse. We have used a quartz lens of 1 m focal length to focus the beam through a 40 $\mu$m diameter pinhole acting as a spatial filter and another 1 m focal length quartz lens to recollimate the radiation to give a parallel beam. Nine 266 nm mirrors at 45° were used to filter out the 800 nm and 400 nm wavelength components from the 266 nm UV pulse. The pulse width of the final 266 nm laser pulse was estimated to be 170 fs (FWHM). The beam was focused onto the target sample using a quartz 40× microscope objective (Partec objective, Numerical Aperture 0.8, working distance 0.8 mm). The energy delivered to the sample was measured using a photodiode cross calibrated against a Spectra Physics model 407A power meter and monitored throughout the experiment. A CCD camera (Point Grey Chameleon USB camera) in conjunction with an f = 15 cm achromatic lens viewing through the same 40× objective and through a turning mirror was used as a sample viewing system to make sure that the sample surface was at the focus of the input beam. In order to obtain a side view of the plasma plume, the emitted plasma light was

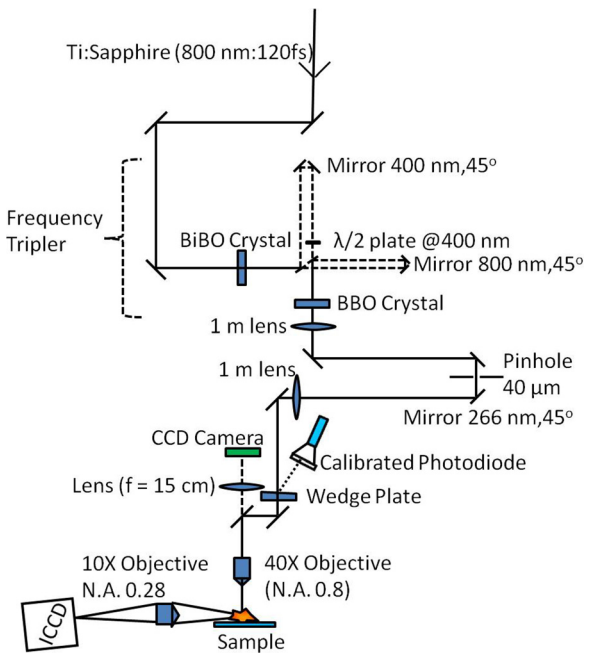


FIG. 1. Schematic of the experimental setup.

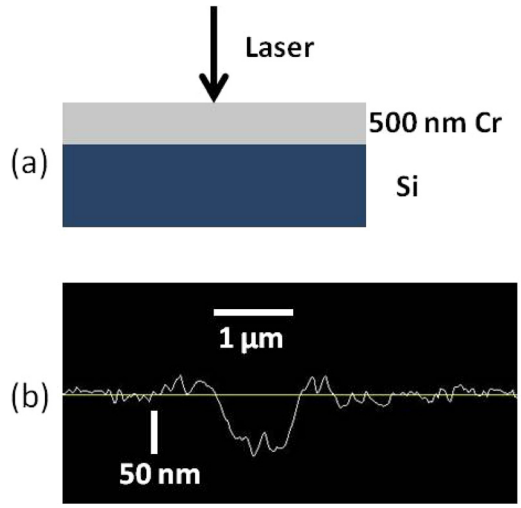


FIG. 2. (a) Schematic of target sample and (b) AFM lineout scan of the single ablation spot at 170 nJ.

imaged onto an ICCD (Andor iStar ICCD) camera using a 10× microscope objective (Mitutoyo, NA 0.28). The microchannel plate gain of the ICCD camera was set to 200 (out of 255) for all the experiments. The targets were mounted in a commercial 3D computer controlled precision micropositioning translation stage (Melles Griot Nanomover). The experiments were performed inside a vacuum chamber with the capability to change the pressure in the system. The gate delay time was set to an accuracy of 0.5 ns relative to the laser pulse. Different gate delays were used to capture plume characteristics at different times. A thin uniform layer of chromium (500 nm) deposited using planar magnetron sputtering on top of a premium silicon wafer was used as the target sample for this experiment, as shown in Fig. 2(a).

## III. RESULTS

A tight focusing objective with very high numerical aperture (N.A. = 0.8) was used to create a micro-ablation region on the target sample. Fig. 2(b) shows the experimentally observed depth profile of the ablation spot using atomic force microscopy (AFM). This shows that the diameter of the crater was ~1 $\mu$m and corresponding depth was ~65 nm. This single shot ablation crater was created using a 170 nJ laser pulse energy. We employed this energy to explore plasma plume structures and their evolution at different background pressures. This particular energy value was chosen to ensure that we had sufficient emission radiation from the plasma plume to characterize the plasma and at the same time the ablation spot is in the range of a micron or less. We also have carried out measurements with different energy values lower than 170 nJ which will be discussed later in the paper. In order to take snapshots at different times, we have varied the gate delay by steps of 5 ns and accumulate the emission from the plasma over an integration time of 5 ns for each exposure. The reported delay times refer to the time from the laser pulse to the end of this gate window. The emission from a single shot ablation plasma was not sufficient to produce a good resolution image. Therefore, we have accumulated 50 single laser shots to produce an image of the

plasma plume. Every laser shot was taken on a fresh target surface and the gate time, gate width, and all other experimental parameters were the same during this accumulation.

### A. Plume images

Plasma plume images were taken at various background pressures of air and at different time delays with respect to the laser pulse. The background pressure values used for the experiment were 0.3 Torr, 2.3 Torr, 5.5 Torr, 18.5 Torr, 29 Torr, 52 Torr, 107 Torr, and at ambient air pressure of 700 Torr. Fig. 3 shows ICCD images of plume expansion at (a) 2.3 Torr, (b) 29 Torr, and (c) at ambient air pressure with a laser pulse energy of 170 nJ. Each of these images was normalized to its own maximum intensity. For the first image, T = 1 ns, we have accumulated 4 ns of time before laser strikes the material surface and 1 ns after that. All of the images employed a 5 ns of gate width. The shape and size of the plume changes significantly as we move from a low background pressure to a high background pressure environment. A forward directed expanding plasma plume with an elongated shape travels quickly out of the target surface at 2.3 Torr. The plasma plume front position reaches ~340 $\mu$m at 46 ns and then the plume disperses into the background medium. The plume front positions were measured at the location where the intensity falls to 10% of the peak intensity

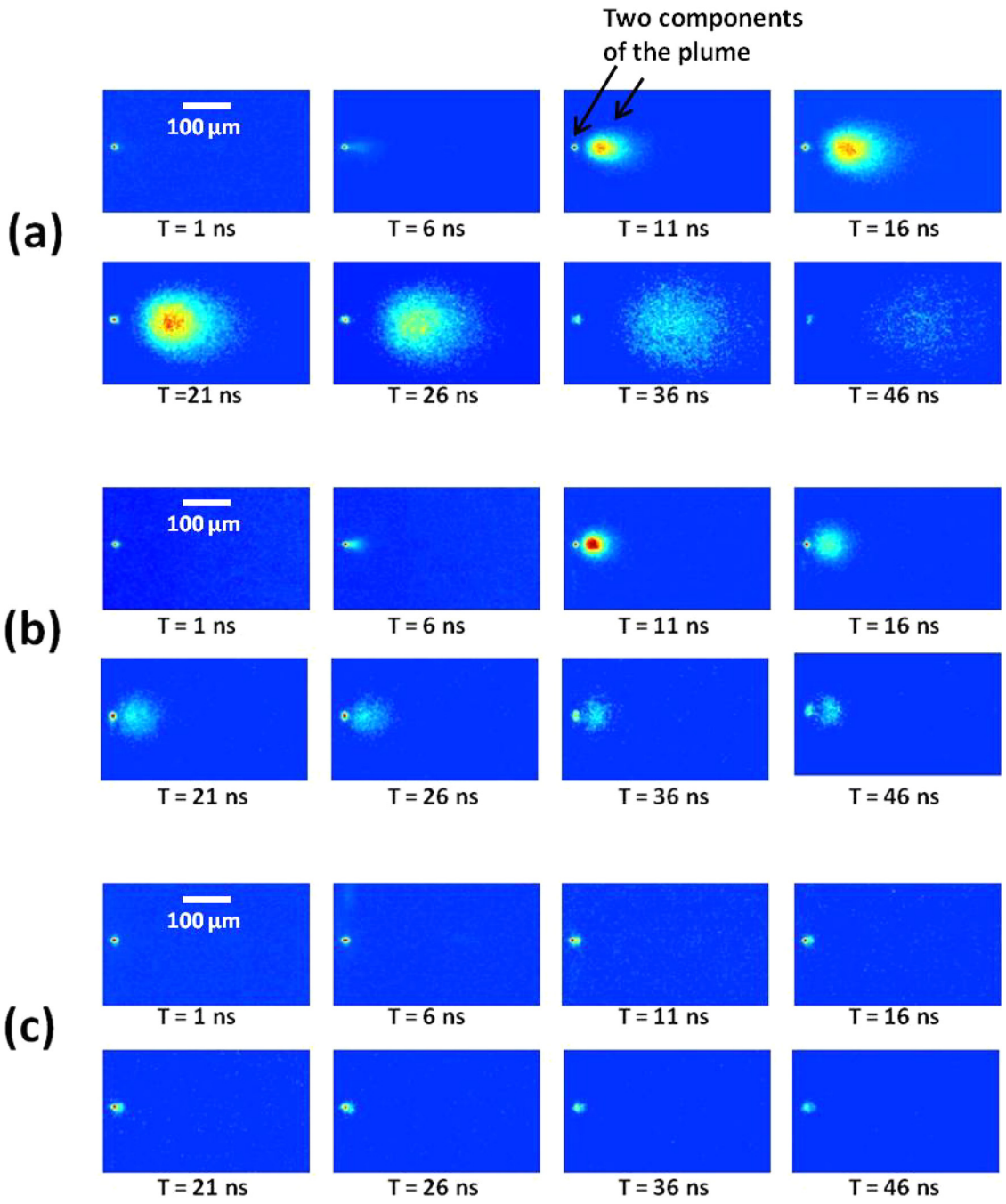


FIG. 3. Temporal evolution of plasma plume at various background pressures: (a) 2.3 Torr, (b) 29 Torr, and (c) at ambient air pressure. The time T denotes the delay after the laser pulse for the end of the 5 ns integration period.

value of any particular plume. At a higher background density of 29 Torr, the expansion is slowed more quickly by collisions with the background gas species and the plasma plume becomes more spherical in shape. The plume front position does not expand past 85 $\mu$m. At ambient air pressure, we see a very tiny plume with little expansion. Fig. 4 shows images of plasma plume taken in the period of 6–11 ns from the onset of laser pulse for various pressures. All images are normalized to their own maximum intensity. This clearly shows how plasma is confined closer to the target surface at high pressure and the plume shape changes from circular to an elongated one at lower pressures. The boundary between the plume front and the surrounding air can be termed as a contact front. A relatively sharp contact front is visible from 5.5 Torr to 107 Torr but it blurs and disappears as pressure decreases. The angular distribution of the plasma plume in femtosecond laser ablation process can be described using the relation $S_\theta = S_0 \cos^n(\theta)$, where $S_0$ defines the particle fluence at the center of the plume and $n$ is a fitting parameter that defines plume anisotropy. We have obtained $n = 5.0 \pm 0.4$ for the case of 107 Torr and $n = 7.5 \pm 0.5$ at 5.5 Torr using the data shown in Fig. 4. This quantitatively describes the change in the plume shape as observed at T = 11 ns when the expansion is already predominantly collisional.

### B. Plume dynamics

Fig. 3(a) shows that a component of the plasma plume is visibly separated from the original plume cloud at T = 11 ns which we refer to as plume splitting. Two arrows in Fig. 3(a) at T = 11 ns show the two components of the expanding plume. If we analyze Fig. 3, splitting of the plasma plume is clearly visible at low pressure (2.3 Torr), barely visible at moderate pressure (29 Torr) and just barely visible at ambient pressure as can also be seen in Fig. 4. This splitting of the plasma plume in two components at low background pressure has been a topic of research using nanosecond[14,24] and femtosecond[18,20] laser pulses by a number of authors. Those experiments showed that the first component is the quickly expanding ionic and atomic plume containing ions and atoms and the second component is primarily filled with slow-moving atomic vapor and nanoparticles of the target sample material. Amoruso *et al.*[25] have shown that the early time expansion ($\tau < 1$ $\mu$s) of a Ni plume at a laser fluence of 0.9 J/cm$^2$ shows ionic and atomic plume characteristics, whereas nanoparticle plume expands at a later time ($\tau > 1$ $\mu$s). They also have shown[18] that the two components of the plume move with a velocity of $\sim 10^4$ and $\sim 10^2$ m/s, respectively, at low pressure. In our case, the plasma lifetime is very small because of low incident energy of our laser pulse. The whole emission process decays away within 60 ns from the time laser strikes the material. Therefore, we could not observe temporally different regimes for the evolution of two detached plumes. The slow part of the plume that appears just above the target sample as soon as laser ablation occurs will be called the surface plume in our subsequent discussion. Fig. 5 shows the contour plot of this part of the plume at (a) 0.3 Torr, (b) 18.5 Torr, and (c) 52 Torr at different times. It can be seen from the figure that the movement of the center of the surface plume is small in the first 21 ns but it reaches 6 $\mu$m (0.3 Torr) and 8.5 $\mu$m (18.5 Torr, 52 Torr) at 56 ns. The velocity can be calculated as $(1.1 \pm 0.2) \times 10^2$ m/s and $(1.5 \pm 0.3) \times 10^2$ m/s for pressures of 0.3 Torr and 52 Torr, respectively, which matches well with the reported slow component expansion velocity from previous studies. However, at 56 ns, the plume may still primarily be in atomic vapor form since it will take some time for the vapor to cool and condense into nanoparticles.

The faster part of the plasma plume region expands and propagates into the background gas very rapidly. Plume propagation can be studied quantitatively by analyzing the position of the plume front as a function of time. The images of the plume clouds were converted into intensity contour plots. The leading surface of the contour where the intensity has a value of 10% its maximum value was taken as the plume front position. This front basically separates the plume cloud from the surrounding medium. The plots of the position of the leading edge of the plume versus time for different ambient background pressures are shown in Fig. 6. Fig. 6(a) shows at very low pressure (0.3 Torr) the plume expands almost freely in the background gas with an average velocity of $0.83 \times 10^4$ m/s. The plume expansion appears to be linear in the early stage of its evolution but the time span of linearity decreases with increasing background gas pressure due to the increasing collisional stopping power at higher pressures, leading to a ballistic expansion time period scaling approximately as the inverse of pressure. At 0.3 Torr, we can use $R_{\mu m} = 12 t_{ns}$ to fit the initial expansion as shown. Propagation is linear until approximately 15 ns and the velocity of the plume decreases thereafter.

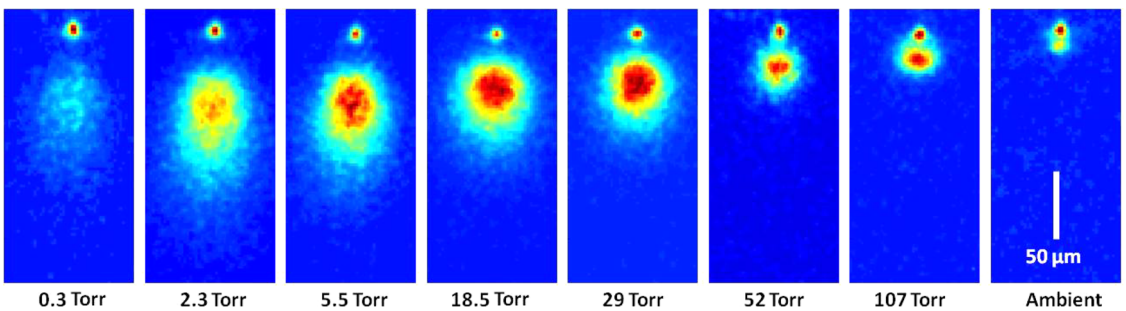


FIG. 4. Images of plasma plume for an accumulation end time of 11 ns from the onset of the laser pulse for various pressures. The laser enters from the bottom.

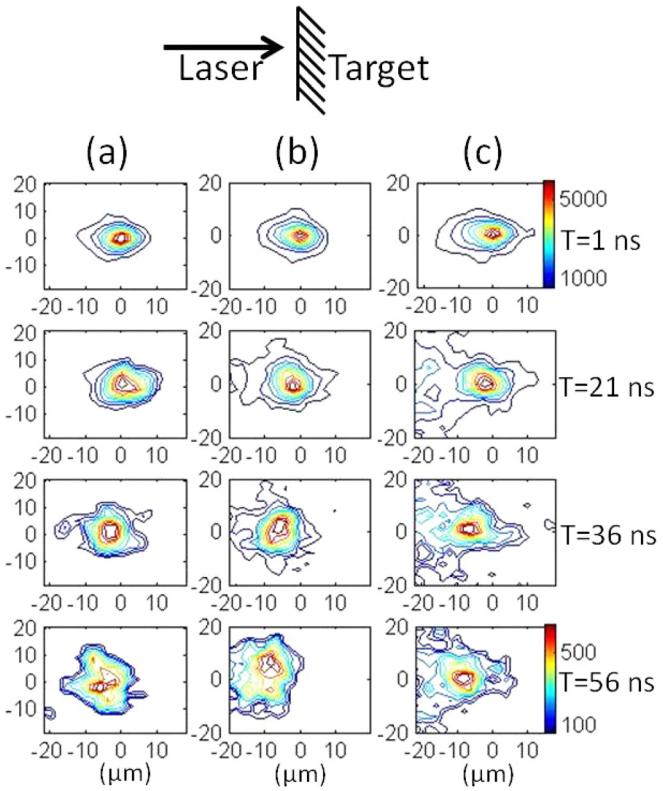


FIG. 5. Contour plot of the slow component plume at background pressures of (a) 0.3 Torr, (b) 18.5 Torr, and (c) 52 Torr. Time T denotes delay after the laser pulse.

Plume expansion and propagation in a collisional background gas can be described with two models. One is the blastwave model and the other one is the drag model. The Sedov-Taylor point source explosion theory[26,27] predicts the expansion of a blast wave in background gas and can be used to determine the dependence of the propagation of plasma plume on the background gas pressure. In this model, the expansion of the plasma plume generates a strong pressure impulse in the background gas generating a strong shockwave that precedes the plasma. The Sedov-Taylor equation[27] states that the blast wave front position $R$ originating from an instantaneous pulsed release of energy is given in the case of spherical symmetry by

$$R = \lambda_0 \left(\frac{E}{\rho}\right)^{1/5} t^{2/5}, \tag{1}$$

where $\lambda_0$ is a dimensionless constant dependent on the specific heat of the gas with a value close to 1, $E$ is the energy released during the explosion which can be taken as the absorbed laser pulse energy (taken as half the incident laser energy), $\rho$ is the density of background gas, and $t$ is the propagation time for the blast wave. We have used this equation to calculate the plume front position at different background gas pressures as shown in Figs. 6(a)–6(d) for 0.3 Torr, 5.5 Torr, 18.5 Torr, and 52 Torr, respectively. It is seen that the blastwave model does fit for the highest density case shown at 52 Torr background pressure but becomes progressively worse at lower pressures. This is due to two factors. The first is that the initial expansion of the energetic ions is ballistic until collisions slow down the initial plasma particles and allow them to couple to a pressure wave in the background gas. Second, the ideal blast wave solution only assumes instantaneous release of energy in the background gas and does not take into account the mass of the ablated particles and the extra momentum that they couple into the expanding gas. Both these factors lead to an increase in the real expansion velocity of the plasma plume. However, as the background pressure increases, the initial ballistic expansion is stopped more quickly and the relative mass injected becomes smaller and smaller relative to the mass of the background gas. Thus, the blast wave model becomes more accurate at the higher pressures of around 50 Torr.

In the second model,[28,29] the plasma plume expands rapidly in the beginning but slows down thereafter until it reaches a limiting expansion distance which is also known as the stopping distance. The drag force created by the background gas molecules results in deceleration of the plasma plume. The motion of the plasma front towards the stopping distance can be expressed in the form of the drag model[28,29]

$$R(t) = R_0(1 - e^{-\beta t}), \tag{2}$$

where $R(t)$ is the distance of the plume edge at time $t$ and $R_0$ is the stopping distance. The damping coefficient $\beta$ indicates the amount of resistance imposed by the background gas to the plasma expansion. Fig. 6 shows the R-t plots for the drag model which has been fit to the plume expansion for 5.5 Torr (b), 18.5 Torr (c), and 52 Torr (d). The stopping distances for different pressures were taken from the experimental plume propagation images. The $R_0$ values were $250 \pm 20\,\mu$m at 5.5 Torr, $130 \pm 20\,\mu$m at 18.5 Torr, and $60 \pm 10\,\mu$m at 52 Torr. The corresponding $\beta$ values are $0.06 \pm 0.01\,\text{ns}^{-1}$ at 5.5 Torr, $0.1 \pm 0.04\,\text{ns}^{-1}$ at 18.5 Torr, and $0.15 \pm 0.06\,\text{ns}^{-1}$ at 52 Torr. The drag model does not apply at very low pressure and thus we have not tried to fit it for the 0.3 Torr case where the plasma moves with a slowly decreasing velocity over the period of observation. By choosing the appropriate coefficients, the drag model fits fairly well for the three higher background pressure cases throughout the plasma plume expansion.

### C. Plume length

Plume length can also be estimated at different background pressures using an adiabatic expansion model[14,30] which prescribes a plume length given by the point where the adiabatically expanding plasma plume pressure equals the background gas pressure. The plasma length is then given by

$$L = A[(\gamma - 1)E]^{1/3\gamma} P_0^{-1/3\gamma} V_i^{(\gamma-1)/3\gamma}, \tag{3}$$

where $\gamma$ is the specific heat ratio of the ablation plume species, E is the absorbed laser energy, $P_0$ is the ambient gas pressure, $V_i$ is the initial heated volume of the plasma, and A is a geometric factor. Normally for ns duration pulses, $V_i$ is taken as $V_i = \upsilon_0 \tau_{laser}(\pi r^2)$, where $\upsilon_0$ is the initial expansion velocity, $\tau_{laser}$ is the laser pulse width, and r is the radius of the spot size, respectively.

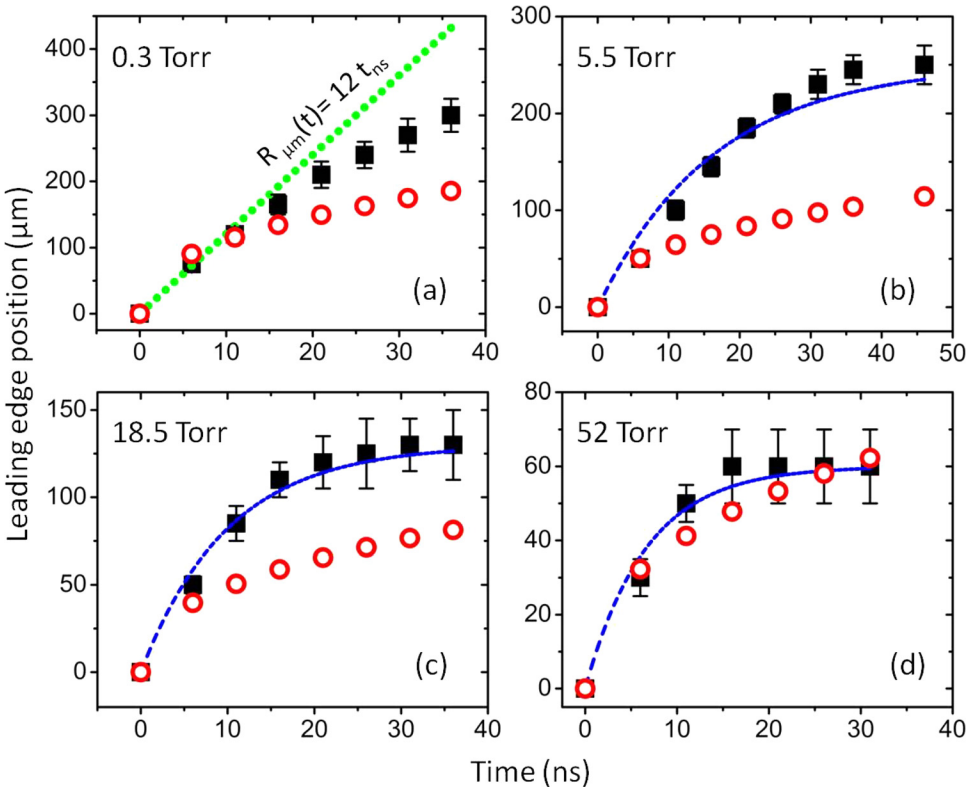


FIG. 6. Position of the leading front of the chromium plasma plume produced in background gas pressure of (a) 0.3 Torr, (b) 5.5 Torr, (c) 18.5 Torr, and (d) 52 Torr obtained from the gated ICCD images at different times. Experimental data points (■), linear fit (●), blastwave calculation (○), and drag model fit (–) are shown with different fitting parameters. For the drag model $\beta = 0.06 \pm 0.01\,\mathrm{ns}^{-1}$ at 5.5 Torr, $\beta = 0.1 \pm 0.04\,\mathrm{ns}^{-1}$ at 18.5 Torr, and $\beta = 0.15 \pm 0.06\,\mathrm{ns}^{-1}$ at 52 Torr

In the present case, we take the initial volume as the conical volume formed by the distance of initial ballistic expansion of the energetic plasma at the measured velocity of $1.2 \times 10^4$ m/s with a cone angle of expansion given by the average cone angle of the plasma plume measured for each different background pressure. The duration of the ballistic expansion period is calculated from the case of 0.3 Torr background pressure where it was found that the expansion was purely ballistic up to a time of ~15 ns. Assuming that the collision time scales inversely with background pressure, this expansion time is given for different pressures by $15(\frac{0.3}{P_{torr}})$ ns. To calculate plume expansion angle $\theta$, we have measured the plume images at different times and taken a best fit of the cone half angle (half width at 10% peak intensity) averaged over all images for a particular gas pressure. We obtained values of $\theta$ of 27°, 31°, 36°, 39°, 43°, and 45° for 2.3 Torr, 5.5 Torr, 18.5 Torr, 29 Torr, 52 Torr, and 107 Torr, respectively. For a conical plume with a spherical leading surface, the geometric factor A can be calculated as[30]

$$A = \left(1 + \frac{1}{\tan\theta}\right)\left(\frac{3\tan\theta}{\pi + 2\pi\tan\theta}\right)^{1/3}, \qquad (4)$$

where $\theta$ is the measured cone half angle. The initial energy, E, can be estimated from absorbed laser energy. The starting optical absorption at 266 nm for chromium metal is 41%.[31] However, as the chromium metal is ionized by the femtosecond laser pulse, the warm dense matter state created will have a different absorption coefficient. Previous reports of absorption show that for femtosecond UV laser pulses, once a plasma is formed, the absorption tends to converge to a value of approximately 50% for different starting materials.[32] Thus, for simplicity, we have assumed an absorption coefficient of 50% giving an absorbed energy of 85 nJ per pulse in our experiment for an incident energy of 170 nJ. The specific heat ratio $\gamma$ was taken as 5/3 for chromium and values of the initial heated volumes $V_i$ were calculated as $3.54 \times 10^{-15}\,\mathrm{m}^3$, $3.58 \times 10^{-16}\,\mathrm{m}^3$, $1.37 \times 10^{-17}\,\mathrm{m}^3$, $4.44 \times 10^{-18}\,\mathrm{m}^3$, $1.02 \times 10^{-18}\,\mathrm{m}^3$, and $1.35 \times 10^{-19}\,\mathrm{m}^3$ for 2.3 Torr, 5.5 Torr, 18.5 Torr, 29 Torr, 52 Torr, and 107 Torr, respectively. Fig. 7 shows the experimental and calculated values of the plume length for different background pressures. Experimental values of plume length are obtained from the ICCD images of the plume. Contour plots of the plume images were analyzed at the time before the plume disperses into the background and the distance measured from the target to the outermost points of the contours where the intensity falls to 10% of its peak intensity value were taken as the plume length.[30,33] The plume length is essentially the same as the plume front position at stagnation point. These values are plotted in Fig. 7. In addition, the length of the plasma emission region defined by distance between the 10% intensity points in the axial direction is also plotted. This is termed as plume emission length. It is seen that at lower pressures the total plume length is bigger than predicted from the adiabatic expansion model while the plume emission length is close to the model predictions. This indicates that at lower pressures the plasma is ejected ballistically into the background gas and then starts an adiabatic type expansion after a significant propagation distance when it becomes collisional. This appears to effectively displace the starting point of the adiabatic expansion away from the target surface.

### D. Plume images near threshold

In order to obtain plume images near the threshold ablation regime, we reduced the laser pulse energy until the images disappeared. We have acquired plasma plume evolution images on the ICCD for different delay times, T. The background pressure was kept at 19 Torr to make the final plume almost circular with a relatively sharp contact front. The minimum energy was 26 nJ for which the laser plasma plume was still visible at this pressure. Laser pulse energies of 26 nJ, 33 nJ, 44 nJ, 71 nJ, and 111 nJ were chosen for the experiment to show how the plasma plume formation and propagation changes with pulse energy. The experimental condition and procedures to obtain images are the same as described earlier. Fig. 8 shows the plume images for laser pulse energies of 26 nJ and 33 nJ. Each of these images is normalized to its own maximum intensity. An estimated half micron diameter focal spot with 26 nJ of laser pulse energy corresponds to an approximate energy fluence of 13 J/cm$^2$ which can be taken as the approximate plasma emission threshold value for our experimental parameters. For an incident energy of 26 nJ, the plasma plume moves to ~50 $\mu$m after 11 ns and disperses outwards after that. At 33 nJ, the plume forms a more circular shape and propagates until 16 ns. The distance covered is 80 $\mu$m in 16 ns which corresponds to a velocity of the plume of $0.5 \times 10^4$ m/s. This is lower than that observed for 170 nJ pulses by approximately a factor of 2 times which is to be expected since the five times lower incident intensity would lead to a colder plasma temperature and lower ion velocity.

Next, we investigated the scaling of integrated emission brightness of the ablation plume as a function of delay time. In order to do this, we have integrated the counts for all the pixels of the plume images minus the background dark image counts. The gain of the ICCD was set at 200 which corresponds to approximately 90 counts for one generated photoelectron. Therefore, we have integrated pixels only which are more than 90 counts to make sure that at least one photoelectron was present. Fig. 9 shows the plot of integrated intensity versus time for different laser pulse energy. The integrated intensity increases with increasing pulse energy as expected. For 26 nJ, the integrated counts reach a maximum at 6 ns and then decrease rapidly. As the pulse energy increases, the maximum integrated brightness was observed at approximately 11 ns. The lifetime of a plasma plume can be approximated as the time when the integrated counts of the plasma plume image drops to (1/e) of its peak value. Using this we can estimate the single pulse plasma lifetime for 26, 33, 44, 71, and 111 nJ energies as 11.5, 18, 19.5, 20, and 22 ns, respectively, for the pressure of 19 Torr.

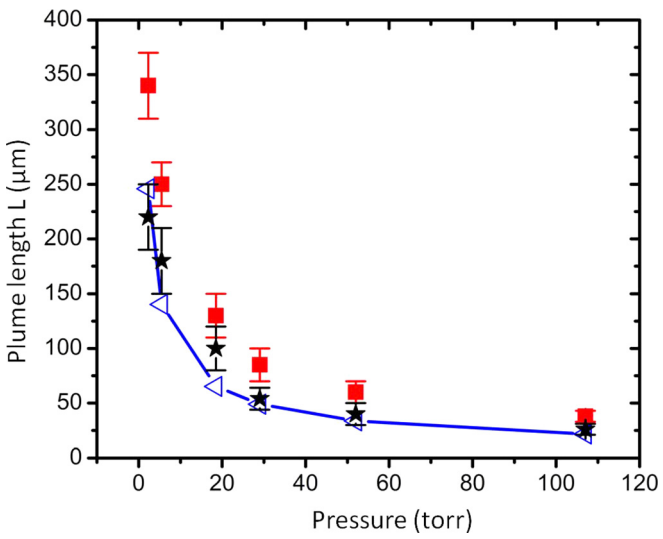


FIG. 7. Plume length $L$ of the chromium plasma at different ambient pressures. Experimental plume length (■), plume emission length (★), and calculated values (-◁)

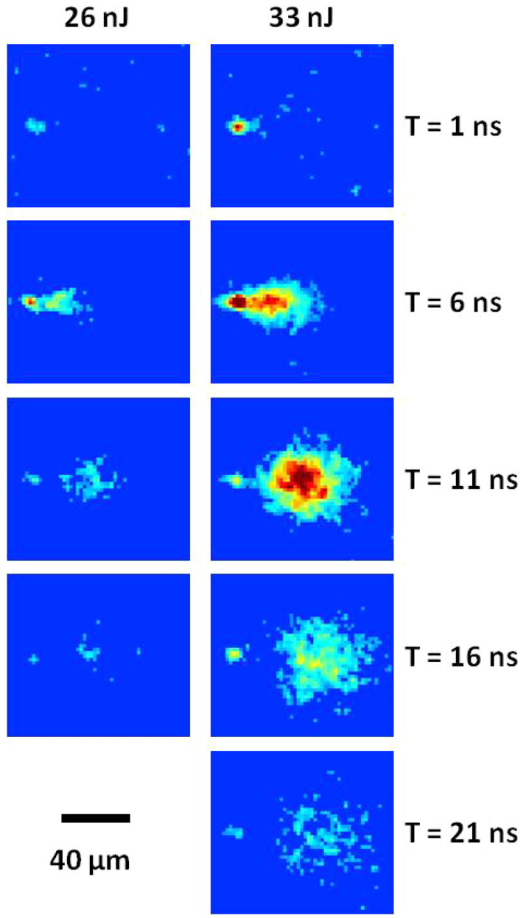


FIG. 8. Temporal plasma plume expansion at 19 Torr background pressure with laser pulse energies of 26 nJ (left) and 33 nJ (right). Time, T, denotes delay after the laser pulse. The laser is incident from the right.

## IV. DISCUSSION

In the present study, we investigate a new regime of plasma plume expansion for very low incident energies in the nanojoule regime. This regime leads to much smaller plasma volumes with shorter plasma lifetimes than in previous studies. However, it is observed that the plasma plume follows the same general behavior as it does for the case of higher incident energies. As shown in Sec. III, this behavior can be broken into four regimes: (1) ballistic expansion, (2) collisional expansion, (3) stagnation, and (4) slow expansion of a surface plume arising from the heated solid target material. The ballistic expansion period is on the order of nanoseconds

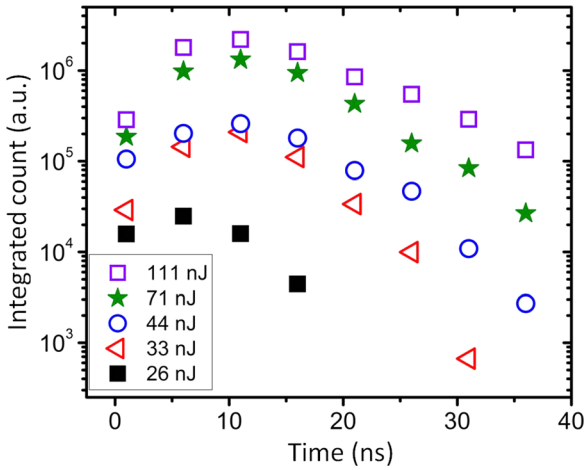


FIG. 9. Integrated intensity counts for the plume images for different laser pulse energies.

to subnanosecond in duration, decreasing with increasing pressure as the collision frequency increases with pressure. The collisional regime can be described by two models, either a simple blast wave model or a collisional drag model. The former is applicable if the expansion is dominated by collisions and is not perturbed by excessive mass injection or a long preceding period of ballistic expansion. These criteria are best satisfied in our case for background pressures of around 50 Torr where the calculated blast wave expansion agreed well with our measured expansion. The collisional drag model is more general and fits all the expansion cases except the lowest background pressure cases where the ballistic expansion dominates. However, it requires appropriate choices of the damping coefficient and stagnation distance for each background pressure. Finally the stagnation distances can be estimated from the expansion distance at which pressure balance is obtained between the adiabatically expanding plasma plume and the background gas. As shown in Fig. 7, good agreement between the measured values of the plasma emission length and the model is obtained assuming conical expansion and an initial volume given by the ballistic expansion distance. It is then useful to compare these results to previously published results obtained at higher laser pulse energies.

Plume splitting into two distinct components with different velocities has been observed by various authors for nanosecond and femtosecond laser pulses with higher incident energy (few $\mu$J or more). We do see similar splitting of plasma plumes into two components with different velocities but the low incident energy and small size of the initial plume restricts the observation of the slow moving component to short time durations over which only a modest amount of expansion is observed. Amoruso *et al.*[25] have shown that the composition of the two parts of the femtosecond laser plasma plume can be determined by the spectral emission of the relevant components. The fast component shows emission due to the atomic species of the target material whereas, self emission of the slow component shows a structureless, broadband, continuum spectrum which is characteristic of hot nanoparticles produced during the event. It is important to note that the spectra and the evolution of nanoparticles were determined at $\tau > 1\,\mu$s, a much longer timescale than our observed period. Thus, our slow expansion plume corresponds to the expansion of hot dense target species which probably will evolve into the nanoparticle plume observed in these previous studies. Previously reported plasma plume shapes are spherical-like for nanosecond laser produced plasmas, whereas, femtosecond pulses show a preferential forward directed expansion of the plasma along the target normal in a low pressure environment.[20,22] This can be explained by the generation of high plasma pressure on the surface at the initial time due to the strong over heating.[22] A strong forward directed velocity component is generated with little resistance from the background neutrals at low pressure. At very low pressure ($1.5 \times 10^{-4}$ Torr), even nanosecond plasmas exhibit such a directed expansion behavior.[15] We observe similar shape changes in plasma plume with different background pressures.

Al-Shboul *et al.*[22] have used 40 fs, 800 nm laser pulses with ~6.9 mJ energy to create a plasma plume that expanded to a stopping distance of ~4.8 mm in 5 Torr background $N_2$ pressure. In our case, the plasma plume has moved a maximum of ~250 $\mu$m at 5.5 Torr background gas pressure where the pulse energy was ~170 nJ. The propagation distance is ~19 times smaller, whereas the pulse energy is $4 \times 10^4$ times smaller in our case compared to theirs. To compare to our result, we can assume a similar supersonic expansion velocity of $1.2 \times 10^4$ m/s during the first 0.9 ns (using the previous estimate given by the expression $15(\frac{0.3}{P_{torr}})$) of the plasma plume expansion and use the focal spot diameter as 100 $\mu$m as reported by them[22] to calculate the initial heated volume in their case. This leads to an initial cylindrical plasma plume volume of $3.39 \times 10^{-13}$ m$^3$ which is ~950 times greater than in our experiment. From Eq. (3), for $\gamma = 5/3$, we can say $L \propto E^{1/5} V_i^{2/15}$ for a fixed expansion angle. Therefore, the ratio of propagation distance can be estimated as 21 times smaller in our case using this equation which is very close to our observed ratio of 19 times.

At low background pressures, past reports have shown that the two components of the laser ablated plasma plume are found to propagate at an average velocities of ~0.8–$2.4 \times 10^4$ m/s (Refs. 18, 20, 25, 29, and 30) and ~1–$5.2 \times 10^2$ m/s (Refs. 18, 25, and 34) for fast and slow components, respectively, for a wide range of pulse energies with nanosecond and femtosecond laser pulses. Although at very low background gas pressure, femtosecond pulses show slightly higher plume propagation velocity than the nanosecond cases, e.g., $2 \times 10^4$ m/s for fs pulses compared to $1.4 \times 10^4$ m/s for ns pulses for Ca(I) species as reported in the literature.[20] In the case of nanojoule laser pulse energies, we have observed similar velocity behavior of the two components of the plasma. Amoruso *et al.*[35] have used MD simulations coupled with a two-temperature model to study the ablation process due to 300 fs laser pulses. The simulations predicted a most probable velocity of $\approx 1 \times 10^4$ m/s for the fast component and $\approx 3 \times 10^2$ m/s for the slow components of the expanding plasma plume into vacuum. The average velocity of the plume front decreases with increasing background pressure.

The evolution of plume propagation with time has been described by the blastwave model and drag model in many of the past experiments. A general form of expression of $R \propto t^n$ for the blastwave model has been used in past to compare experimental data in nanosecond[12,14,36] and femtosecond[20,37] laser plasma cases where $n \sim 0.4$. The pressure value where this model fitted best was reported as ~11 Torr with ~40 mJ, 10 ns (FWHM) laser pulses by Dyer and Sidhu[12] and 15 Torr with ~47.5 mJ, 8 ns (FWHM) laser pulses by Mahmood *et al.*,[15] respectively. In our case, the blastwave model has been used with the exact values of each parameter and assuming an estimated 50% energy absorption. The plasma plume expansion can be temporally divided into different regimes: initial ballistic expansion, collisional expansion, and stagnation. For the lowest pressure case of 0.3 Torr, a predominantly ballistic expansion is observed as would be expected when there is little collisional coupling. For the collisional regime, the time span for a pure blast wave expansion is short due to the initial period of ballistic expansion and the fairly rapid onset of stagnation. Therefore, deviation from an ideal blast wave solution is expected at the lower background pressures where the ballistic expansion period represents a significant fraction of the overall plume expansion time but at the same time good agreement is observed at a background pressure of 52 Torr.

In all but the lowest pressure cases, a drag force model can be applied with a good agreement to the measured data. In most cases reported earlier, the drag model fits better at all background pressures specifically on or above ~10 Torr.[14,36] This model depends on the value of $\beta$, the damping coefficient at a particular gas pressure. As $\beta$ determines the amount of resistance by the background pressure, it changes with different pressure values as shown earlier. From the previous studies, various values of $\beta$ were estimated as $0.0003\,ns^{-1}$, $0.002\,ns^{-1}$, and $0.04\,ns^{-1}$ for the background pressures of 0.1 Torr,[28] 1.3 Torr,[29] and 10 Torr,[36] respectively. We also have found that $\beta$ changes from $0.06\,ns^{-1}$ to $0.15\,ns^{-1}$ as background gas pressure changes from 5.5 Torr to 52 Torr. We can expect that $\beta$ scales approximately linearly with the background pressure since it depends on the damping of the expansion in the background gas. Such an approximate scaling is seen from the past references and our $\beta$ values falls close to these values irrespective of the fact that the references have used high energy nanosecond laser pulses in comparison to our fs, nanojoule pulse. The higher value of this damping coefficient $\beta$ at higher background pressures would be due to higher resistance exerted by the neutrals of the background gas on the expanding plasma plume. This increased resistance causes confinement of the plasma near the target surface at high pressure.

## V. CONCLUSION

In this work, plasma plume characteristics have been investigated in the regime of low incident laser pulse energies appropriate for precision micromachining and high resolution microLIBS. The spatio-temporal evolution of the plasma plume at different ambient pressures shows that the plume shape changes from spherical to forward directed as the pressure changes from high to a low value. The angular distribution of the plumes has been characterized both in the terms of conical width and best fit cosine power law functions. Splitting of plasma plume into two distinct slow and fast components was observed at pressures of ~100 Torr and below. These two different components of the plume have been identified as the rapid ion driven expansion plume and the much slower atomic vapor plume which eventually would condense into a nanoparticle cloud as observed in the previous experiments at late time. The velocity of the ionic and atomic vapor plumes were $1.2 \times 10^4$ m/s and $\sim 1 \times 10^2$ m/s, respectively. At pressures of ~50 Torr, a blast wave model fitted the plume expansion fairly well. At lower pressures of 5–50 Torr, an expansion drag model fitted the data fairly well with appropriate choice of the drag coefficient $\beta$ in the range of $0.06\,ns^{-1}$ to $0.15\,ns^{-1}$. At very low pressures, the plume propagation is initially almost ballistic with a constant velocity and then slows down in time. The maximum plume length was calculated based on a pressure balance model and compared well to the experimentally obtained values at higher background pressures. At lower pressures, it appears that the adiabatic expansion starts from a displaced point in the background plasma leading to a plume emission length which is close to the value predicted by the adiabatic expansion model. Plume images were also studied down to the emission threshold fluence of approximately $13\,J/cm^2$ and the emission lifetimes found to scale from 11 ns to 22 ns for energies of 26–111 nJ, respectively.

Overall the behavior could be described well with a combination of models including ballistic expansion, blast wave expansion, collisional drag expansion, and pressure stagnation of the expanding plume. The dominant behavior depends on the pulse energy, the background pressure, and time of observation. This description is consistent with observations of plume dynamics previously reported for higher laser pulse energies. A more complete understanding of the expansion dynamics would require numerical modeling of the expansion processes over all the above regimes. However, this is left for future work. It is also expected that these results will be useful in application areas of such low energy plasmas such as femtosecond pulsed laser deposition, precise laser micromachining, laser induced breakdown spectroscopy, and production of nanoparticles.

## ACKNOWLEDGMENTS

The authors wish to acknowledge funding for this research from the Natural Sciences and Engineering Research Council of Canada.

[1]E. Millon, O. Albert, J. C. Loulergue, J. Etchepare, D. Hulin, W. Seiler, and J. Perrière, J. Appl. Phys. **88**, 6937 (2000).
[2]A. A. Melaibari and P. Molian, J. Appl. Phys. **112**, 104303 (2012).
[3]R. R. Gattass and E. Mazur, Nature Photon. **2**, 219 (2008).
[4]G. D. Valle, R. Osellame, and P. Laporta, J. Opt. A: Pure Appl. Opt. **11**, 013001 (2009).
[5]S. E. Kirkwood, M. T. Taschuk, Y. Y. Tsui, and R. Fedosejevs, J. Phys.: Conf. Ser. **59**, 591 (2007).
[6]R. Fedosejsvs, Y. Tsui, Z. Chen, and S. Banerjee, *Nano-Fabrication Techniques and Principles*, edited by M. Stepanova and S. Dew (Springer-Verlag/Wien, 2012), p. 301.

[7]B. Tan and K. Venkatakrishnan, Opt. Express **17**(2), 1064 (2009).
[8]D. W. Hahn and N. Omenetto, Appl. Spectrosc. **64**(12), 335 (2010).
[9]I. V. Cravetchi, M. T. Taschuk, Y. Y. Tsui, and R. Fedosejevs, Anal. Bioanal. Chem. **385**, 287 (2006).
[10]S. Yalcin, Y. Y. Tsui, and R. Fedosejevs, J. Anal. At. Spectrom. **19**, 1295 (2004).
[11]K. Kagawa and S. Yokoi, Spectrochim. Acta, Part B **37**(9), 789 (1982).
[12]P. E. Dyer and J. Sidhu, J. Appl. Phys. **64**(9), 4657 (1988).
[13]D. B. Geohegan and A. A. Puretzky, Appl. Phys. Lett. **67**(2), 197 (1995).
[14]S. S. Harilal, C. V. Bindhu, M. S. Tillack, F. Najmabadi, and A. C. Gaeris, J. Appl. Phys. **93**(5), 2380 (2003).
[15]S. Mahmood, R. S. Rawat, M. Zakaullah, J. J. Lin, S. V. Springham, T. L. Tan, and P. Lee, J. Phys. D: Appl. Phys. **42**, 135504 (2009).
[16]M. Cirisan, J. M. Jouvard, L. Lavisse, L. Hallo, and R. Oltra, J. Appl. Phys. **109**, 103301 (2011).
[17]S. Yalcin, Y. Y. Tsui, and R. Fedosejevs, IEEE Trans. Plasma Sci. **33**(2), 482 (2005).
[18]S. Amoruso, R. Bruzzese, X. Wang, and J. Xia, Appl. Phys. Lett. **92**, 041503 (2008).
[19]T. Donnelly, J. G. Lunney, S. Amoruso, R. Bruzzese, X. Wang, and X. Ni, J. Appl. Phys. **108**, 043309 (2010).
[20]S. Canulescu, E. Papadopoulou, D. Anglos, T. Lippert, M. J. Montenegro, S. Georgiou, M. Döbeli, and A. Wokaun, Appl. Phys. A **105**, 167 (2011).
[21]Z. Wu, X. Zhu, and N. Zhang, J. Appl. Phys. **109**, 053113 (2011).
[22]K. F. Al-Shboul, S. S. Harilal, and A. Hassanein, Appl. Phys. Lett. **100**, 221106 (2012).
[23]T. Donnelly, J. G. Lunney, S. Amoruso, R. Bruzzese, X. Wang, and X. Ni, Appl. Phys. A **100**, 569 (2010).
[24]R. F. Wood, J. N. Leboeuf, K. R. Chen, D. B. Geohegan, and A. A. Puretzky, Appl. Surf. Sci. **127–129**, 151 (1998).
[25]S. Amoruso, R. Bruzzese, C. Pagano, and X. Wang, Appl. Phys. A **89**, 1017 (2007).
[26]Sir G. Taylor, Proc. R. Soc. London, Ser. A **201**, 159 (1950).
[27]L. I. Sedov, *Similarity and Dimensional Methods in Mechanics* (CRC Press, Boca Raton, 1993).
[28]D. B. Geohegan, Appl. Phys. Lett. **60**(22), 2732 (1992).
[29]S. S. Harilal, C. V. Bindhu, M. S. Tillack, F. Najmabadi, and A. C. Gaeris, J. Phys. D: Appl. Phys. **35**, 2935 (2002).
[30]P. E. Dyer, A. Issa, and P. H. Key, Appl. Phys. Lett. **57**(2), 186 (1990).
[31]J. H. Weaver and H. P. R. Frederikse, "Optical properties of metals and semiconductors," in *CRC Handbook of Chemistry and Physics*, 74th ed. and subsequent printings (CRC Press, Boca Raton, Florida, 1986), p. 12–118.
[32]R. Fedosejevs, R. Ottmann, R. Sigel, G. Kühnle, S. Szatmári, and F. P. Schäfer, Appl. Phys. B **50**, 79 (1990).
[33]V. Berardi, S. Amoruso, N. Spinelli, M. Armenante, R. Velotta, F. Fuso, M. Allegrini, and E. Arimondo, J. Appl. Phys. **76**, 8077 (1994).
[34]S. Noël, J. Hermann, and T. Itina, Appl. Surf. Sci. **253**, 6310 (2007).
[35]S. Amoruso, R. Bruzzese, X. Wang, N. N. Nedialkov, and P. A. Atanasov, J. Phys. D: Appl. Phys. **40**, 331 (2007).
[36]A. K. Sharma and R. K. Thareja, Appl. Surf. Sci. **243**, 68 (2005).
[37]N. Zhang, X. Zhu, J. Yang, X. Wang, and M. Wang, Phys. Rev. Lett. **99**, 167602 (2007).